Phytoplankton "Missing" Absorption in Marine Waters: A Novel Pigment Compensation Model for the Packaging Effect

Yu Huan[1], Deyong Sun[1], Shengqiang Wang[1], Muhammad Bilal[1], Hailong Zhang[1], Zhongfeng Qiu[1], and Yijun He[1]

[1]Nanjing University of Information Science & Technology

November 22, 2022

Abstract

The packaging effect of phytoplankton pigments is sometimes capable of accounting for over half of the variability in the phytoplankton absorption coefficient (aph) in oceanic waters. Given the significance of aph in many marine biogeochemical and environmental processes, exploring the packaging effect on absorption properties thus becomes a crucial task. In the present study, two pigment compensation models for quantifying the packaging effect are developed for Case I and Case II waters, respectively, based on high-performance liquid chromatography (HPLC)-derived pigments and aph data from the NOMAD and the marginal seas of China. As a critical quantity in developing our models, phytoplankton "missing" absorption is derived by subtracting the reconstructed aph without the packaging effect from the measured aph. Our proposed models use the established relationships between "missing" absorption and specific absorption coefficients of pigment groups without the packaging effect to quantify pigment group concentrations. Validation using independent in situ data sets demonstrates that great improvements are achieved for the quantification of the packaging effect, especially for waters under abnormal packaging effect conditions. Applying the proposed models to satellite data displays the spatial distributions of the packaging effect in the Atlantic Ocean and the marginal seas of China, as delegates of Case I and II waters, respectively. The generated spatial distribution demonstrates a rule that the packaging effect intensity positively covaries with chlorophyll-a distribution. The findings of this study exhibit a capability of mapping a spatial distribution of the packaging effect from satellite observations for the first time.

Phytoplankton "Missing" Absorption in Marine Waters: A Novel Pigment Compensation Model for the Packaging Effect

Yu Huan[1], Deyong Sun[1, 2], Shengqiang Wang[1, 2], Muhammad Bilal[1, 2], Hailong Zhang[1, 2], Zhongfeng Qiu[1, 2], and Yijun He[1, 2]

[1] School of Marine Sciences, Nanjing University of Information Science & Technology, Nanjing, China

[2] Jiangsu Research Center for Ocean Survey Technology, NUIST, Nanjing, China

Corresponding author: Deyong Sun (sundeyong@nuist.edu.cn)

Key Points:

- Our developed pigment compensation model improves the current underestimation to the phytoplankton absorption coefficient in solution
- Characterization of the unidentified phytoplankton pigment group increases the accuracy of quantifying the pigment packaging effect
- Achieving the satellite inversion to the packaging effect that enable to generate its spatial and temporal pattern for the first time

Abstract

The packaging effect of phytoplankton pigments is sometimes capable of accounting for over half of the variability in the phytoplankton absorption coefficient (a_{ph}) in oceanic waters. Given the significance of a_{ph} in many marine biogeochemical and environmental processes, exploring the packaging effect on absorption properties thus becomes a crucial task. In the present study, two pigment compensation models for quantifying the packaging effect are developed for Case I and Case II waters, respectively, based on high-performance liquid chromatography (HPLC)-derived pigments and a_{ph} data from the NOMAD and the marginal seas of China. As a critical quantity in developing our models, phytoplankton "missing" absorption is derived by subtracting the reconstructed a_{ph} without the packaging effect from the measured a_{ph}. Our proposed models use the established relationships between "missing" absorption and specific absorption coefficients of pigment groups without the packaging effect to quantify pigment group concentrations. Validation using independent in situ data sets demonstrates that great improvements are achieved for the quantification of the packaging effect, especially for waters under abnormal packaging effect conditions. Applying the proposed models to satellite data displays the spatial distributions of the packaging effect in the Atlantic Ocean and the marginal seas of China, as delegates of Case I and II waters, respectively. The generated spatial distribution demonstrates a rule that the packaging effect intensity positively covaries with chlorophyll-a distribution. The findings of this study exhibit a capability of mapping a spatial distribution of the packaging effect from satellite observations for the first time.

Plain Language Summary

The packaging effect is a bio-optical phenomenon that enables to weaken the phytoplankton absorption coefficient, further causing the variability of remote sensing reflectance, especially in the blue waveband. However, the accurate quantification to the packing effect is greatly limited by commonly-existing underestimation to the phytoplankton absorption coefficient in solution by previous methods. To solve this problem, our study took six major pigment groups into account and developed two pigment compensation models for Case I and Case II waters, respectively. We found that the compensation of the major pigment groups could increase the accuracy of the packaging effect quantification, such as the contribution of the sixth pigment group at the green waveband that was seldom considered well in the previous studies. The satellite-derived spatial distribution on the packaging effect in the marginal seas of China and the Atlantic Ocean confirms a common rule, that is, the packaging effect increases along with the increasing chlorophyll-a concentration. We suggest that future ocean color satellite products should cover the packing effect, and assess its influence on the variability of the bio-optical parameters in waters.

1 Introduction

The packaging effect of phytoplankton pigments enables phytoplankton to distinctly change their absorption, and the effect commonly exists in Case I or Case II ocean waters, especially in water with large phytoplankton and high chlorophyll-a (Chla) concentrations (Nelson et al., 1993; Bricaud et al., 2004; Ciotti et al., 2002; Jena, 2017; Lewis et al., 2016; Wang et al., 2014).

By influencing phytoplankton absorption, the packaging effect is further capable of affecting the variability in the remote sensing reflectance (R_{rs}) in the visible light band. Previous studies have reported that errors in R_{rs} introduced by the packaging effect may lead to significant uncertainties in retrieving Chla from satellite observations (Alcântara et al., 2016; Jena, 2017). It can be inferred that the tasks associated with a_{ph} and Chla suffer from the potential influence of the packaging effect, such as phytoplankton primary production (Boatman et al., 2019; Claustre et al., 2005; Lewis et al., 2016) and phytoplankton functional types (Bracher et al., 2009; Hirata et al., 2008; Mouw et al., 2017, 2010; Xi et al., 2020). Thus, accurate characterization and quantification of the packaging effect have become a significant and urgent problem for many aspects of oceanographic research.

The phytoplankton absorption coefficient normalized to Chla is known as a specific absorption coefficient (a_{ph}^*), which is subject to the packaging effect (Brewin et al., 2019; Jena, 2017; Kirk, 1975; Morel & Bricaud, 1981). Berner et al. (1989) reported that the packaging effect could cause 51–57% variability in a_{ph}^*. According to previous studies (Berner et al., 1989; Kirk, 1983), factors influencing the packaging effect can be generally divided based on two sets of characteristics. The first set includes the size, shape, number of phytoplankton cells, chloroplasts, and even the distribution of chloroplasts in phytoplankton cells. The second set includes the nature of thylakoid membranes, including their degree of stacking and optical properties, which enables them to decide how much optical radiation energy can be available to the chloroplast. Owing to the relative stability of the second set of factor characteristics, previous studies have mainly focused on the first set of factor characteristics, and the size and concentration of phytoplankton cells are also available from satellite observations at higher spatiotemporal resolutions (Brewin et al., 2015; Ciotti et al., 2006; Devred et al., 2006, 2011; Uitz et al., 2006; Wang et al., 2018).

The packaging effect is traditionally quantified and defined as a ratio of in situ measured a_{ph} to that under a dissolved disperse state ($a_{ph,sol}$) (Bricaud et al., 1995, 2004; Morel & Bricaud, 1981; Nelson et al., 1993). Theoretically, the phytoplankton absorption coefficient could be reconstructed from the sum of different pigments and their specific absorption spectra. Bidigare et al. (1990) observed and reported the unpackaged specific absorption coefficients of several major pigment groups, namely, Chla, chlorophyll-b (Chlb), chlorophyll-c (Chlc), photosynthetically active carotenoids (also called photosynthetic carotenoids, PSC), and photoprotectant carotenoids (also called photoprotecting or photoprotective carotenoids, PPC), together with two types of phycobilins from pure pigment. Based on the specific absorption coefficients, the reconstructed a_{ph} values were then compared with those in situ measured a_{ph} sample values collected from different times and depths of the study area and found that the packaging effect was inconspicuous in open oceanic waters. Nelson et al. (1993) reported that the packaging effect cannot be obvious if $a_{ph,sol}(\lambda) < a_{ph}(\lambda)$. Woźniak et al. (1999, 2003) obtained five major, specific absorption spectra using the Gaussian function decomposition method based on in situ measured samples from the Atlantic Ocean and Baltic Sea and further regarded the "Ocean version" for $a_{ph,sol}$ derivation. Notably, the phycobilins showed an important effect on obtaining $a_{ph,sol}$. Unlike other pigments, phycobilins are dissolvable in water and difficult to extract by commonly used methods such as HPLC (Ficek et al., 2004;

Woźniak et al., 2007). This increases the difficulty of accurately quantifying the contribution of phycobilins to the $a_{ph,sol}$. Ficek et al. (2004) presented a method to estimate the phycobilin content by taking the sixth pigment group, namely, the unidentified group (UP), and recorded its absorption-specific coefficient based on several phycobilin absorption-specific spectra referred to previous studies (Bidigare et al., 1990; Tarchevsky, 1977, Grabowski, 1984, Hall & Rao, 1999); this updated method was subsequently regarded as the "Baltic version" for accurately obtaining the $a_{ph,sol}$ for Case II waters. It is a substantial breakthrough that provides the sixth pigment group to compensate for the absorption contribution from the part that HPLC cannot detect. The method to estimate the UP by Ficek et al. (2004) is only based on the assumption that a mass-specific integral absorption for the UP is equal to the similar integral absorption for phycobilins. Thus, the concentration of UP must be determined based on several specific absorption spectra of different phycobilins. However, it is not useful to use UP as a constant for all types of seawater under different conditions. Therefore, another starting point of our study was to seek an empirical and easier method to estimate UP concentration. A recent study reported the specific absorption spectra of 30 phytoplankton pigments in the dissolved state (Clementson & Wojtasiewicz, 2019). Compared to the "Ocean version" and "Baltic version", these spectra provide more detailed pigments and unpackaged specific absorption coefficients, but phycobilins are still not covered, indicating that they need to be investigated.

The abovementioned spectrum reconstruction method is not the only way to obtain $a_{ph,sol}$ in oceanic waters. Assuming that phytoplankton cells are symmetrically spherical and optically soft particles, the packaging effect can be expressed as the absorption efficiency function (Morel & Bricaud, 1981) and finally transformed as a function of the product of specific absorption spectra (a^*), the intracellular Chla concentration (C_I), and cell diameter (d). Therefore, quantifying the three variables is an important yet challenging task. When the specific absorption coefficients were obtained using the Gaussian function, also discussed above, two empirical methods were used to establish the relationship between C_Id and Chla for the Atlantic Ocean and Baltic Sea in previous studies (Ficek et al., 2004; Woźniak et al., 1999). These two empirical models were subsequently regarded and built for Case I and Case II waters (Woźniak et al., 2007; Ye et al., 2019). The performances using the existing relationship models with other seas are probably uncertain and need to be evaluated.

The model based on the absorption efficiency function has the advantage of a theoretical background, but some key parameters are still obtained through empirical models. On the other hand, the spectrum reconstruction method has fewer variables and is much easier to perform. The most frequent abnormal condition was that the retrieved packaging effect based on the spectrum reconstruction method may be larger than 1 (no packaging effect) in some cases (Bricaud et al., 2004; Nelson et al., 1993), which means that the reconstructed $a_{ph,sol}$ is less than that measured in situ.

In this paper, we assumed that the "missing" absorption of $a_{ph,sol}$ may be caused by the underestimation of pigment groups and the development of several compensation equations for major pigment groups, including the UP group, was used to improve the illogical packaging effect based on the local data set. The performance of each model was validated by independent

data sets, and satellite remote sensing was applied to analyze the potential space-time features of the packaging effect in different oceans.

2 Data and methods

2.1 HPLC-derived phytoplankton pigments and a_{ph} data sets

In this study, four in situ measured data sets with HPLC-derived phytoplankton pigments and a_{ph} were collected in different oceans: (1) the marginal seas of China (Data set A), (2) the Atlantic Ocean (Data set B), (3) the South Atlantic Ocean (Data set C), and (4) the Pacific Ocean (Data set D). A detailed description of them is as follows (Figure 1):

Data set A

The marginal seas of China, consisting of the Yellow Sea, Bohai Sea (YBS) and East China Sea (ECS), are the marginal seas in the western Pacific, typically optically complex Case II waters. The methods of water sample collection and follow-up data treatment were based on steps in previous studies (Aiken et al., 2009; Sun et al., 2017, 2019). Data set A included five cruises in the marginal seas of China, namely, the ECS cruise in Spring 2016, the YBS cruise in Summer 2016, the ECS cruise in Autumn 2016, the YBS cruise in Winter 2016, and the ECS cruise in Spring 2017. This data set included a total of 183 samples with a Chla range of 0.1–3 mg m^{-3}, which was subsequently used for building the pigment compensation model.

Data set B

The NASA bio-Optical Marine Algorithm Data set (NOMAD) is a global, high-quality, in situ observation data set, publicly available for algorithm development and ocean-color satellite validation. It covers many bio-optical variables and can be obtained from the US National Aeronautics and Space Administration (NASA) website (Version 2.a, 18/07/2008, https://seabass.gsfc.nasa.gov/wiki/NOMAD). In this study, the absorption coefficient of the total suspended particles, $a_p(\lambda)$; and absorption coefficient of the detrital particles, $a_d(\lambda)$; and HPLC-derived pigments were used for our subsequent model establishment and comparison. A total of 277 in situ measured samples were selected according to the quality control method of Aiken et al. (2009) and were divided into two parts based on the fuzzy c-means clustering function (FCM), namely Data set B-I (n=203) and Data set B-II (n=74). The Data set B-I measurements were mainly distributed in the Atlantic Ocean, while the Data set B-II measurements were located in coastal waters with Chla concentrations above 1 mg m^{-3}. Data set B-I was subsequently used for model development in Case I waters, and Data set B-II was used for model validation in Case II waters.

Data set C

The South Atlantic Ocean Data set was developed from the POLARSTERN cruise ANT-XXVIII/3 in January and February 2012 and available from the PANGAEA (Data Publisher for Earth & Environmental Science) website (https://doi.pangaea.de/10.1594/PANGAEA.819614). The cruise collected samples in seven layers at different depths from the surface to 100 m along a longitudinal sample section. In this

study, only the surface water samples (n=190) were utilized. A detailed description of the data measurement is in a previously published work (Soppa et al., 2013) and the PANGAEA website. This data set was then used for model validation for Case I waters.

Data set D

The Pacific Ocean data set (n=106) was collected from 42.628°N to 19.249°S in the West Pacific Ocean, during the SONNE cruise SO202/2 in Autumn 2009 (Zindler et al., 2013) (https://doi.pangaea.de/10.1594/PANGAEA.804525). The measurements of phytoplankton pigment and absorption coefficient data can be found in Zindler et al. (2013) and Taylor et al. (2011). The current study used this data set to validate the performance of the developed model for Case I waters, together with other data sets.

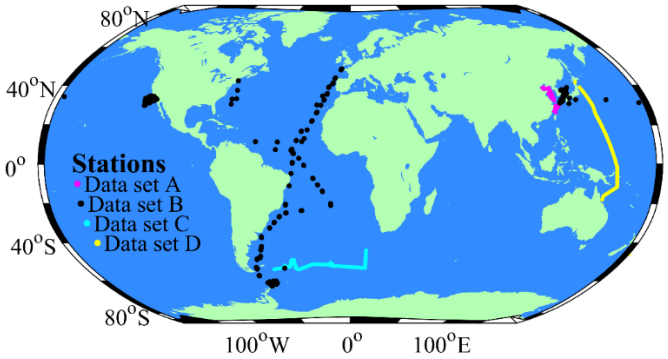

Figure 1. Locations of in situ data collection used in this study. Data set A was collected in the marginal seas of China, Data set B distributes mainly in the Atlantic Ocean, Data set C is from the South Atlantic Ocean, and Data set D was obtained in the Pacific Ocean.

2.2 Satellite data

The Suomi National Polar-orbiting Partnership (SNPP) is the first satellite of the US National Polar-orbiting Operational Environmental Satellite System (NPOESS) and a member of the US Earth Observing System (EOS), providing long-term climate research and real-time weather forecasting. It was successfully launched on 28 October in 2011, carrying a Visible Infrared Imaging Radiometer Suite (VIIRS) sensor. VIIRS is a successful ocean color satellite sensor that has accumulated a large amount of high-quality data since its launch. In this study, VIIRS level-3 year-averaged (for the 2018 year) data at a 9 km resolution, including a_{ph} from quasi-analytical algorithm (QAA) (Lee et al., 2002), a_{ph_QAA} (443); absorption due to dissolved organic matter from QAA, a_{dg_QAA} (443); backscattering coefficient of particulate from QAA, b_{bp_QAA} (443); and chlorophyll-a concentration from OCX algorithm (Chl_{ocx}) (O'Reilly et al., 2000), were obtained from the NASA ocean color data website (https://oceandata.sci.gsfc.nasa.gov/VIIRS-SNPP).

2.3 Quantification of the pigment package effect

The pigment package effect, $Q_a^*(\lambda)$, is conventionally defined as a ratio of in situ measured $a_{ph}(\lambda)$ to $a_{ph,sol}(\lambda)$ (Eq. 1).

$$Q_a^*(\lambda) = a_{\mathrm{ph}}(\lambda) / a_{\mathrm{ph,sol}}(\lambda) \quad (1)$$

where λ is the wavelength in the visible light bands. In general, $a_{\mathrm{ph,sol}}(\lambda)$ can be reconstructed through the sum of multiple pigment absorptions (Ciotti et al., 2002; Ficek et al., 2004; G. Wang et al., 2018) using the product of specific absorption coefficients and pigment concentrations (Eq. 2).

$$a_{\mathrm{ph,sol}}(\lambda) = \sum \left[a_i^*(\lambda) C_i \right] \quad (2)$$

where C_i is the concentration of the i-th pigment and $a_i^*(\lambda)$ represents the specific absorption coefficient of the i-th pigment measured in the dissolved state. In principle, more pigments are required in Eq. (2) for accurate estimation of $a_{\mathrm{ph,sol}}(\lambda)$. In this study, both versions, i.e., the "Ocean version" (Woźniak et al., 1999) and "Baltic version" (Ficek et al., 2004) algorithms, were applied to accurately estimate $a_{\mathrm{ph,sol}}$ in Case I and II waters, respectively. The flowchart of this study is shown in Figure 2.

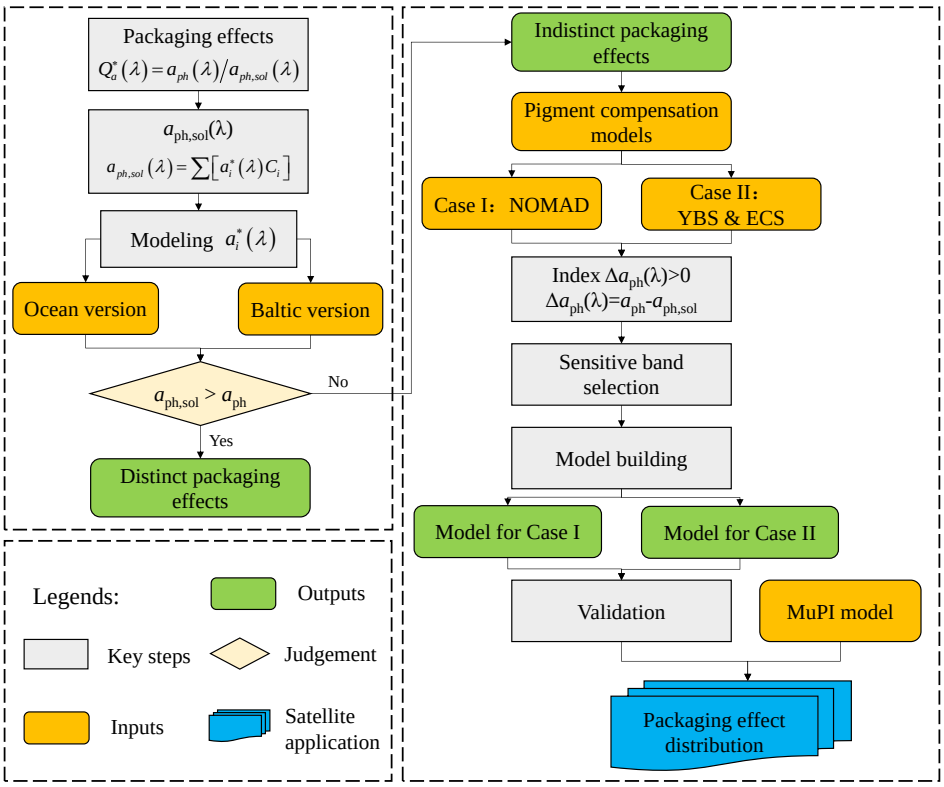

Figure 2. Schematic flow chart showing the developed model for reconstructing the packaging effect. Different colors, as shown in the legend, represent different processes, including inputs, key steps, judgment, and satellite application.

2.4 Performance metrics

Model establishment and satellite data processing were carried out using MATLAB software (MathWorks Inc., Natick, MA, USA). To evaluate the performance of the developed models, two indicators were used in the study, including the determination coefficient, R^2, and root mean square error, *RMSE*. *RMSE* was calculated as follows:

$$RMSE = \sqrt{\frac{1}{n}\sum_{i=1}^{n}\left(x_i - y_i\right)^2} \quad (3)$$

where x_i and y_i are the measured and model retrieved values in i-th sample, respectively. n refers to the sample number.

3 Pigment compensation model for the packaging effect

3.1 Model development

Two in situ data sets, representing Case I and Case II waters, were first used to generate the absorption difference (Δa_{ph}) in the visible light bands between a_{ph} and $a_{ph,sol}$, based on the abovementioned "Ocean version" and "Baltic version" methods. The Δa_{ph} was then regarded as the "missing" absorption of phytoplankton. A previous study reported that unavailable pigment measurements (such as phycobilins) would have an important influence on the "missing" absorption (Bricaud et al., 2004), which provided a basis for our study to attribute the "missing" absorption to the underestimation of the pigments' contribution.

The $\Delta a_{ph}(\lambda)$ distribution in the marginal seas of China and the Atlantic Ocean is listed in Figure 3. In the marginal seas of China (Figure 3a), the wavebands at 490 nm, 520 nm, and 676 nm were selected as a reference to analyze the properties of the positive "missing" absorption, which indicated the absorption contribution from certain pigment groups. For instance, the number of samples under Δa_{ph} (520) > 0 in the cyan line was a total of 144, which was the largest among the other conditions, and the positive peak at approximately 520 nm implied a lack of absorption from the UP group. The combination of $\Delta a_{ph}(520) > 0$ and $\Delta a_{ph}(676) > 0$ (n=68) on the blue dotted line (Figure 3a) coincided very well with the purple lines of $\Delta a_{ph}(676) > 0$ (n=71), and the number was only approximately half of that under $\Delta a_{ph}(520) > 0$ (n=144). Notably, the positive peak at 676 nm was mainly from Chla. On the other hand, the combination number of Δa_{ph} (490) > 0 and Δa_{ph} (676) > 0 (n=46) was 23 samples less than that of Δa_{ph} (490) > 0 (n=69), which indicates the discordance among PSC, PPC, and Chla. Considering all these positive peaks, we concluded that the underestimation of the UP group occurred more frequently than that of the other pigment groups, and the underestimate of the PSC and PPC groups occurred next most frequently. This result was normal for the UP group because the reconstruction process did not consider this group. That is, in comparison to Chla, PSC and PPC were much more influenced by the packaging effect. On the other hand, some typical pigment groups could represent certain species, so the difference between $\Delta a_{ph}(\lambda)$ may have indirectly revealed the diverse phytoplankton communities in the data sets here.

In addition, the averaged $\Delta a_{ph}(\lambda)$, calculated by the "Ocean version" method based on NOMAD data (Data set B-I), appeared to have a narrow amplitude of the spectra than that in Figure 3a and was all greater than 0 among the visible light wavebands. This result implies that the "missing" absorption was more distinct in Case I waters than in Case II waters, similar to the results in Bricaud et al. (2004). Four reference wavebands (i.e., 455 nm, 489 nm, 520 nm, and 665 nm) were selected for our new models. The distribution of each condition was close and even overlapped with each other in yellow and red wavebands (Figure 3b). The discrepancies

of $\Delta a_{ph}(\lambda)$ in the different water regions indicated that the establishment of specific models for each case was necessary for accurately quantifying the packaging effect (Figure 3a and b).

In general, the positive $\Delta a_{ph}(\lambda)$ peak in Figure 3a and b had a consistent feature when the wavelength increased, especially at approximately 520 nm and 675 nm. The UP group had an important absorption contribution in the yellow and green wavebands. Even though the positive peak at approximately 520 nm was smoothed easily after adding the UP group according to the specific absorption coefficient of the UP group in the "Baltic version", those peaks in the blue and red wavebands, similar to $\Delta a_{ph}(443)$ and $\Delta a_{ph}(676)$, still existed. Thus, the only quantification for the UP group was still not enough to eliminate the positive $\Delta a_{ph}(\lambda)$ peak in other wavelengths, when the other five pigment groups also needed to be compensated, and using more reference wavebands needed to be considered.

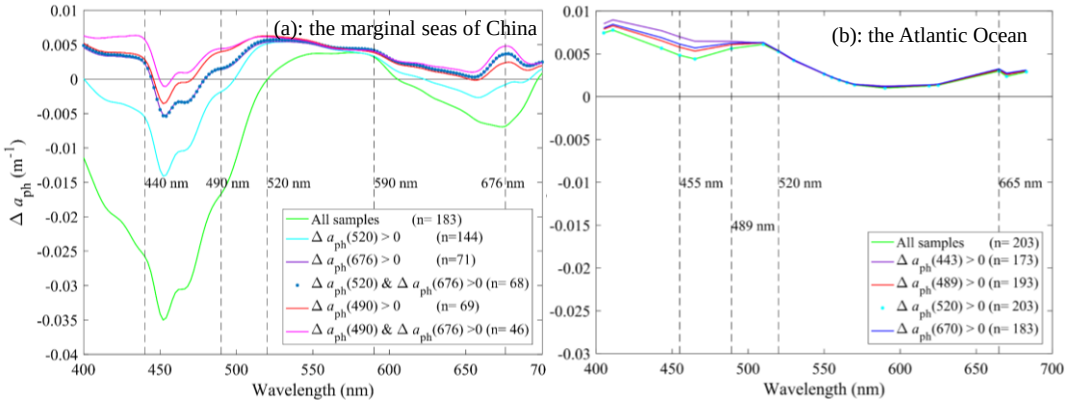

Figure 3. Averaged differences in visible wavebands between inversed and in situ measured $a_{ph}(\lambda)$ values based on the "Baltic version" (a) and "Ocean version" (b) methods. The colored lines represent the errors under different conditions.

After combining those positive peaks with the specific absorption coefficients of each pigment group in both the Baltic and Ocean versions, several wavelengths were selected to build equations to estimate the "missing" term of each pigment group in Table 1. Some slight differences existed in the selection of wavebands, which were mainly at centers of the blue waveband because many pigment groups have absorption peaks in this range. PSC and PPC showed obviously close peak contributions and were assumed to contribute the same at 490 nm in the marginal seas of China. The "missing" pigments at 520 nm almost belonged to the UP group because only the UP group had a peak at approximately 520 nm according to the specific absorption spectra reported in Ficek et al. (2004). Notably, the specific absorption coefficients of Chlb at 590 nm showed similar values to the weak peak of Chlc. Therefore, both peaks were considered contributors at 590 nm. Finally, the positive $\Delta a_{ph}(676)$ was principally responsible for the compensation of Chla concentrations. The retrieval equations were as follows:

$$\Delta a_{ph}(\lambda_i) = \sum_{j=1}^{n} a^*_{ph,j}(\lambda_i) \times \Delta C_j \quad (4)$$

where i is the i-th band; j is the j-th pigment group; $a^*_{ph,j}(\lambda_i)$ is the specific absorption coefficient of the j-th pigment group at the i-th band; ΔC_j is the corresponding "missing"

concentration of the j-th pigment group.

The quantization method for $\Delta a_{ph}(\lambda)$ is another process for successfully obtaining the concentrations of pigment groups. Here, due to the limitation of data resources, $\Delta a_{ph}(\lambda)$ was retrieved as a specific function of the Chla concentration in Case I and Case II waters. The equation coefficients are shown in Table 1, together with the validation error indexes (R^2 and *RMSE*). The retrieval equations performed better in the blue and green wavebands than in the red waveband in both cases, where R^2 decreased from approximately 0.7 to 0.4. Access to $\Delta a_{ph}(\lambda)$ by Chla or other ocean color parameters is a step for further satellite applications.

Table 1

The specific absorption values and equation fitting coefficients of six pigment groups responding to Δaph(λ) at different wavelengths.

Type	Wavelength	Pigments (mg m^{-3})						Δa_{ph} (m^{-1})			
	(nm)	Chla	Chlb	Chlc	PSC	PPC	UP	a	b	R^2	*RMSE*
Model for Case I waters[a]	455		0.08183	0.06882				0.02498	0.6533	0.65	0.0029
	465			0.06780		0.08560		0.02243	0.7209	0.69	0.0028
	489				0.03450	0.07530		0.01459	0.76	0.75	0.0017
	520						1.94E-03	0.00482	0.3636	0.49	0.0014
	665	0.01122	0.02423					0.00700	0.6139	0.24	0.0037
	670	0.02135						0.00798	0.8256	0.44	0.0023
Model for Case II waters[b]	440	0.03372		0.04855				0.00294	0.00644	0.68	0.0058
	490	-			0.05586	0.06793		0.00206	0.00329	0.67	0.0038
	520						1.94E-03	0.00034	0.00518	0.58	0.0044
	590		0.00744	0.00767				0.00010	0.00333	0.48	0.0040
	676	0.02369						0.00187	0.00525	0.58	0.0044

Note. [a]: $\Delta a_{ph}(\lambda)$=a*Chla^b; [b]: $\Delta a_{ph}(\lambda)$=a*Chla^2+b*Chla.

3.2 Model validation

Independent data sets were used to validate the performance of the new models for the South Atlantic Ocean (Data set C), the Pacific Ocean (Data set D), and coastal waters (Data set B-II) for Case I and Case II waters. The improved packaging effect (blue mark) based on our established models was compared with that (magenta mark) without pigment compensation in the coastal waters (Figure 4a-d), South Atlantic Ocean (Figure 4e-h), and the Pacific Ocean (Figure 4i-l). Note that the packaging effects calculated in Figure 4 were all dependent on the "Ocean version" (Case I waters) and "Baltic version" (Case II waters), and our new models adjusted the concentrations of the major pigment groups in the "Ocean version" and "Baltic

version". Thus, the packaging effect in the abnormal state ($Q_a^*(\lambda) > 1$) was transformed to normal ($0 < Q_a^*(\lambda) < 1$).

The packaging effect distributed in Case II waters (Figure 4a-d) showed a good improvement in Chla < 3 mg m^{-3}, especially at 520 nm, where the mean ratio (the number of stations with significant Q_a^* to that of the total stations in a certain Chla range) increased from 70% to 100%. Data set B-II is a part of the NOMAD data set, which had a high Chla concentration. Therefore, the original ratio in the magenta solid line was as high as 1, where Chla > 4 mg m^{-3}. That is, $a_{ph,sol}$ was no longer less than the in situ measured a_{ph} under a high Chla environment, even when influenced by the packaging effect. However, the "missing" absorption of those samples still needed to be revised, as the strong packaging effect is significant for further research.

Validation for Case I water was carried out using Data set C (the South Atlantic Ocean, Figure 4e-h) and Data set D (the Pacific Ocean, Figure 4i-l). The Chla concentration of Data set C ranged from 0.1 to 7.0 mg m^{-3}, similar to that of NOMAD. As expected, the revised Q_a^* in the South Atlantic Ocean showed comprehensive improvements in different wavebands (Figure 4e-h), where the most significant improvements were observed in the blue waveband. The ratio of the effective packaging effect at 455 nm (Figure 4e) was nearly 100%, even at low Chla concentrations. The ratio was approximately 100% when Chla > 4 mg m^{-3}, which was very close to that in Case II waters (Figure 4a-d). This result indicates that the quantification of the packaging effect at low Chla concentrations was more difficult than that at high Chla concentrations because the packaging effect had a greater possibility of being abnormal.

On the other hand, the packaging effect during the Pacific Ocean cruise (Data set D) was constructed through our proposed new model for Case I waters, together with the "Ocean version" method. In Figure 4i-l, we found that Q_a^* on the magenta line had a similar distribution as that in Figure 4a-d, which was within a reasonable range (0–1), and one difference was that the packaging effect in the Pacific Ocean was closer to 1 (approximately no packaging effect), except 520 nm. This result was consistent with those of Bidigare et al. (1990), where the pigment packaging effect was minimal in open-oceanic phytoplankton. The pigment compensation model for Case I waters performed well at 520 nm, where the blue line along the whole Chla-axis had a higher ratio (>90%) than that of the magenta line; this is additional strong evidence for the necessity of estimating UP, especially in open oceanic waters.

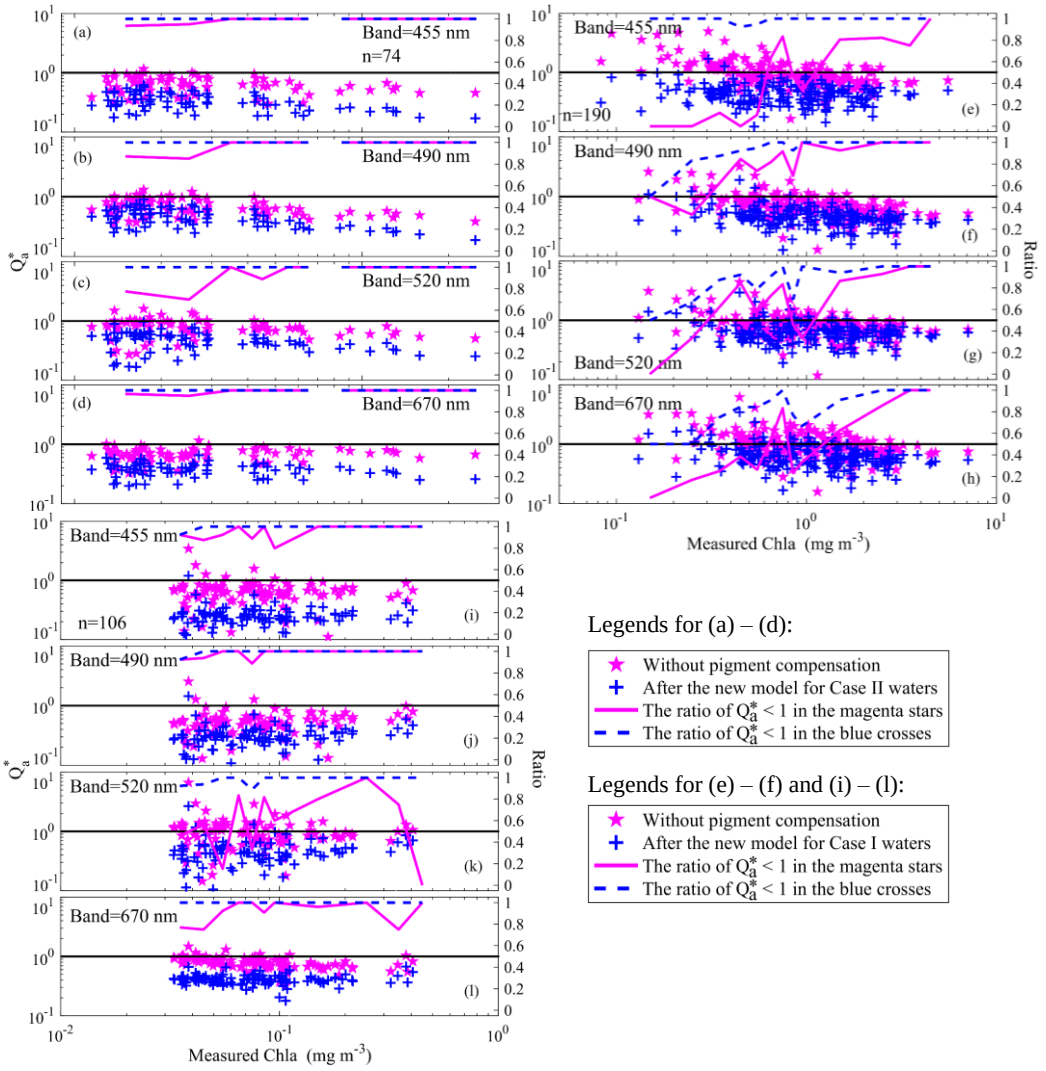

Figure 4. A comparison of the results between the original and revised Q_a^*. (a-d): Data set B-II based on the model for Case II waters in coastal waters; (e-h): Data set C based on the model for Case I waters in the South Atlantic Ocean; (i-l): Data set D based on the model for Case I waters in the Pacific Ocean.

3.3 Application to VIIRS satellite data

The inversion of five major pigment groups, including Chla, Chlb, Chlc, PSC, and PPC, was accomplished through the multi-pigment inversion model (MuPI, Wang et al., 2018; Loisel et al., 2018). To simplify the optimization processes of MuPI, two unknown variables at λ_0 nm, namely, $b_{bp}(\lambda_0)$ and $a_{dg}(\lambda_0)$, were available from the satellite products, and another unknown variable, the peak magnitude of the Gaussian curve at λ_1 nm, namely, $a_{Gau}(\lambda_1)$, was estimated through the Chla satellite product. Finally, the remaining two unknown quantities, namely, the peak magnitude of the Gaussian curve at λ_2 nm, $a_{Gau}(\lambda_2)$, and the spectral decay constant for the absorption of detrital and dissolved materials, S, were obtained using the least-squares method. Here, monthly VIIRS-JNNP satellite data, including $a_{ph\_QAA}(443)$, Chl_{ocx}, $b_{bp\_QAA}(443)$, and $a_{dg\_QAA}(443)$ products at 9 km spatial resolution, were available from the Ocean Color Data Website and used to map the spatial distributions of packaging effects in the

marginal seas of China and the Atlantic Ocean. Twelve monthly satellite data products in 2018 were averaged to an annual mean. Figure 5 demonstrates the spatial distribution of Q_a^* at the blue (443 nm) waveband for the annual average in 2018, together with the Chla isopleth (black solid line) in the marginal seas of China (Figure 5a) and the Atlantic Ocean (Figure 5b).

The $Q_a^*(443)$ in the marginal seas of China shows more variation compared to that in the Atlantic Ocean (Figure 5b), which may have been caused by a large range of Chla concentrations in coastal waters. In general, an increasing latitudinal trend in $Q_a^*(443)$ from north to south was observed in addition to a decreasing Chla concentration, and this negative relationship appeared in the southern coastal area of the Shandong Peninsula and the western coastal areas of the Korean Peninsula. On the other hand, the slope of $Q_a^*(443)$ in the ECS matched well with the Chla isopleth, yet it still showed uncertainty in some highly turbid waters, such as the Subei shoal.

By comparison with that in Figure 5a, $Q_a^*(443)$ showed a consistent trend in most areas of the Atlantic Ocean (Figure 5b). In coastal waters, a strong packaging effect (approximately 0.2) covered the areas where Chla > 0.5 mg m^{-3}. There were two peaks of $Q_a^*(443)$, where a lower center (approximately 0.6) and a higher center (approximately 0.9) were located in the ocean at approximately 0–20°N and 0–30°S, respectively. The higher center was more coincident with the Chla center, where the lower center had a southeastern position ahead relative to the Chla isopleth of 0.05 mg m^{-3}. This phenomenon indicates that the phytoplankton concentration may also lead to the variation in the packaging effect. Note that the relationship between the packaging effect and Chla concentration showed a positive correlation, which has also been reported by other studies (Nelson et al., 1993; Bricaud et al., 2004; Malerba et al., 2018). On the other hand, even though the Chla concentration in the Atlantic Ocean was lower than that in the marginal seas of China, the $Q_a^*(443)$ in the Atlantic Ocean (Figure 5b), with a Chla variation under 0.1 mg m^{-3}, did not have the weakest packaging effect (Q_a^*=1).

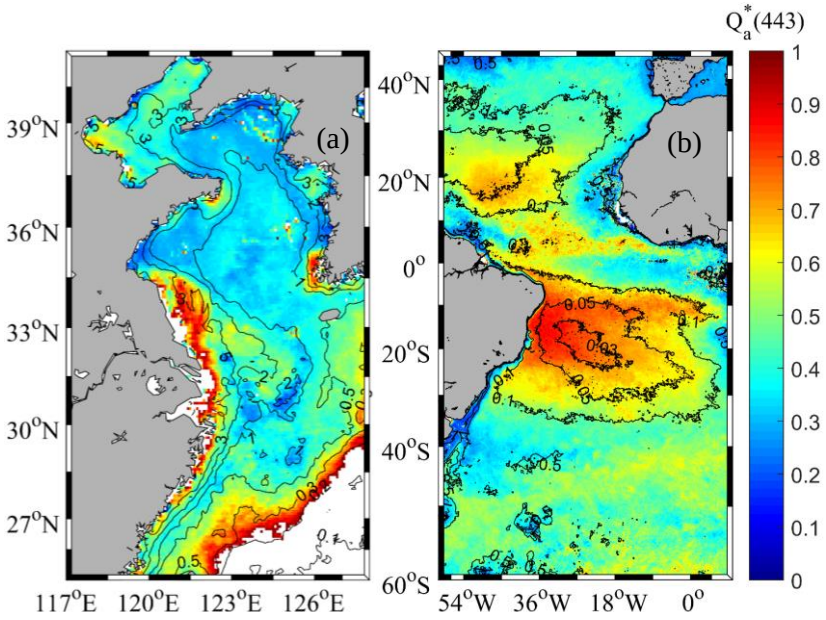

Figure 5. Annual mean (2018) of the packing effect at the 443 nm waveband in the marginal seas of China (a) and the Atlantic Ocean (b). Black lines overlaid on the figures refer to the

isopleth for Chla concentration distribution. Blank regions imply abnormal value distributions that are removed.

4 Discussion

4.1 Pigment distribution in different oceans

Our established pigment compensation models were probably influenced by the pigment concentration distribution. As shown in Figure 6a-e, the distribution of five major pigment groups, including Chla, Chlb, Chlc, PSC, and PPC, can be divided into three types according to the fit lines overlaid. The first type focused on Chla, Chlc, and PSC (Figure 6a, c, and d). A coincident feature was that the frequency peaks for Chla, Chlc, and PSC distribution showed similar shapes and concentration-value centers. The Chla, Chlc, and PSC pigment groups of the NOMAD data set revealed bimodal distribution characteristics. The left peak (approximately 0.2, 0.004, and 0.03 mg m^{-3} for Chla, Chlc, and PSC, respectively) was closer to that of the Pacific Ocean than that of the other data sets, while the right peak was closer to that of the marginal seas of China and the South Atlantic Ocean than that of Data set D. The pigment compensation model for Case I waters was developed by using Data set B-I, with a Chla range of 0.2–1 mg m^{-3}, yet the Chla frequency peak in the Pacific Ocean was located at a range of 0.05–0.2 mg m^{-3}. This may have caused a biased estimation by the model for Case I waters in the Pacific Ocean. The second type was specific to the Chlb distribution (Figure 6b), where a distinct difference from the first type was that Chlb had a nearly coincident area between the South Atlantic Ocean and the Pacific Ocean data set at approximately 0.01 mg m^{-3}. However, there was another peak at approximately 0.1 mg m^{-3} for the Chlb distribution in the South Atlantic Ocean (approximately 0.05–0.2 mg m^{-3}). For the third type, four data sets showed a similar distribution where the PPC distribution peak was 0.05–0.2 mg m^{-3} (Figure 6e). In short, compared to the other pigment groups, Chla had the highest proportion of the total pigment concentration and played a dominant role in modeling the packaging effect. Thus, the Chla distribution shows potential for indicating the packaging effect. Note that our model for Case I waters may generate biased estimations in some regions of the Pacific Ocean (Data set D) with most Chla concentrations below 0.2 mg m^{-3}.

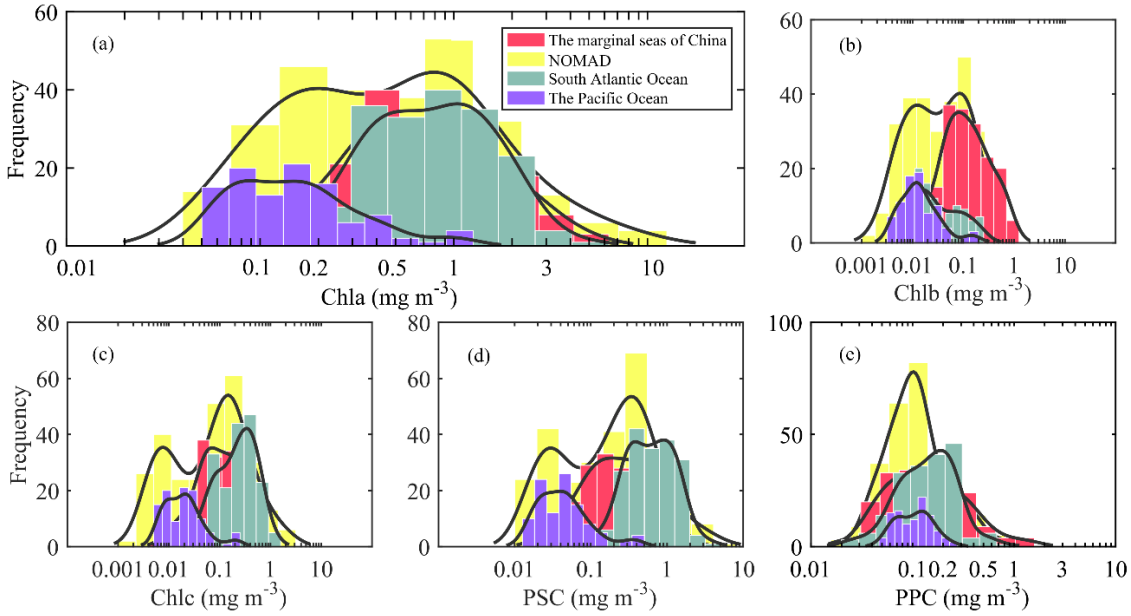

438

439 **Figure 6.** Histogram showing the frequency distribution of in situ measured Chla, Chlb,
440 Chlc, PSC, and PPC in the four sea areas. (a): the marginal seas of China (n=183); (b):
441 NOMAD (n=277); (c): the South Atlantic Ocean (n=190); and (d): the Pacific Ocean
442 (n=106). The black lines denote the normal distribution curves.

443 4.2 Uncertainty analysis of pigment compensation model-derived $Q_a^*(520)$

444 Our developed pigment compensation models generally improved the quantification of the
445 packaging effect in Case I or Case II waters, yet a potential limitation was an inaccurate
446 quantification of the packaging effect at the green waveband, such as $Q_a^*(520)$, when other
447 wavebands performed well. The model-derived $Q_a^*(520)$ in this study sometimes showed an
448 abnormal distribution (>1) in a certain number of samples. The first reason this abnormal
449 distribution has occurred is that it may be attributed to the influence of the UP group that mainly
450 contributed to the green waveband. The specific absorption coefficient of the UP group used in
451 this study was from that reported in Ficek et al. (2004), and there was no sufficient validation
452 of its specific absorption in the marginal seas of China; this scenario may have introduced
453 uncertainty to the quantification of $Q_a^*(520)$. Second, the UP group mainly consisted of
454 phycobilins (Bidigare et al., 1990; Ficek et al., 2004). We did not truly measure its
455 concentration but used an empirical relationship (between $\Delta a_{ph}(520)$ and Chla) to estimate its
456 concentration. Therefore, the model-derived $Q_a^*(520)$ showed greater uncertainties than those
457 of other wavebands.

458 Here, we analyzed the Chla distribution under conditions where the packaging effect
459 quantification was abnormal after performing our models. Those outliers were selected using
460 a differentiation criterion (i.e., $Q_a^*(520) > 1$) in the marginal seas of China (Data set A) and the
461 Atlantic Ocean (Data set B-I) (Figure 7); the Chla ranges of those two data sets showed similar
462 distributions , namely, 0.1 to 2 mg m^{-3} and 0.08 to 2 mg m^{-3}, respectively. The majority of the
463 samples (~82%) in the marginal seas of China fell within 0.2–1 mg m^{-3} (Figure 7a), whereas
464 the same distribution in the Atlantic Ocean (Figure 7b) had approximately 73.91% of points

distributed in the range of 0.1–0.4 mg m^{-3}. Therefore, the underestimation of the reconstructed $a_{ph,sol}$ at 520 nm wavelength appeared within a range of 0.1–1 mg m^{-3}. The abnormal distribution ($Q_a^*(520) > 1$) decreased rapidly when the Chla was close to 1 mg m^{-3} in Case II waters (the marginal seas of China); at the same time, they also decreased in Case I waters (the Atlantic Ocean) where the Chla was close to 0.1 mg m^{-3}. The potential reason for the abovementioned underestimation is that the packaging effect at 520 nm wavelength showed different degrees of variation between Case I and Case II waters. The packaging effect in green waveband may have decreased more from the influence of other pigment groups due to the increasing pigment concentration, but the influence was not distinct at low pigment concentrations, similar to that in the Pacific Ocean.

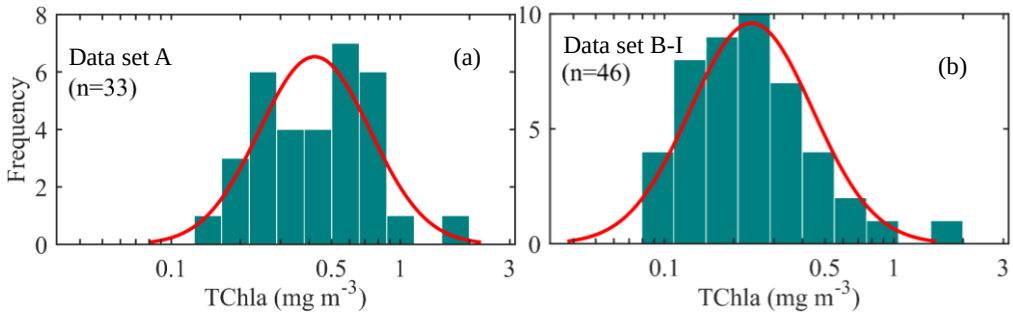

Figure 7. The frequency distribution of in situ measured Chla where $Q_a^*(520) > 1$ after performing our compensation model in the marginal seas of China (a) and the Atlantic Ocean (b). The red lines denote the log-normal distribution fitting curves.

4.3 Implications for future work

Accurate quantification of the packaging effect is significant for evaluating its influence on phytoplankton absorption coefficients and other oceanic variables (Alcântara et al., 2016; Berner et al., 1989; Jena, 2017; Nelson et al., 1993). Our compensation models decreased the possibility of abnormal packaging effect appearance, which was based on the spectrum reconstruction method with in situ pigment and phytoplankton absorption data sets in Case I and Case II waters. Therefore, future research on the packaging effect could be explored for related factors, such as a relationship between the packaging effect and phytoplankton size structure and their influence on other bio-optical quantities. On the other hand, the input parameters for generating spectral and temporal distributions of the packaging effect through satellite observations still exhibited uncertainty to some extent, such as concentrations of the major pigment groups, especially in coastal waters (He et al., 2012).

5 Conclusions

This study develops novel pigment compensation models to quantify the packaging effect for Case I and Case II waters. The models demonstrated here enable us to improve the approach of estimating the packaging effect and distinctly decrease the appearance of abnormal cases with $Q_a^* > 1$. Important progress in our models was characterizing the contribution of the UP group to the phytoplankton absorption coefficient under solvent conditions, which greatly increased the accuracy of the packaging effect quantification, especially in the green waveband.

Our new model for Case II waters performed well under conditions of 0.2 < Chla < 4 mg m^{-3}, and the model for Case I waters performed well at Chla > 0.1 mg m^{-3}. Applying our developed models to satellite data generated the spatial distribution of the packaging effect in the marginal seas of China and the Atlantic Ocean. The satellite-derived results followed a conventional rule well, that is, the higher the Chla concentration is, the stronger the packaging effect. The findings of this study provide an incentive to obtain significant knowledge on the changes in phytoplankton absorption in oceanic waters and further lay a foundation for exploring many related marine biogeochemical processes.

Acknowledgments

This research was jointly supported by the National Natural Science Foundation of China (No. 41876203, 41576172), the National Key Research and Development Program of China (No. 2016YFC1400901), the Jiangsu Six Talent Summit Project (No. JY-084), the Qing Lan Project (No. R2019Q07), the open fund of State Key Laboratory of Satellite Ocean Environment Dynamics, Second Institute of Oceanography (No. QNHX1812), the startup foundation for introducing the talent of NUIST (2019R058), and Science and technology innovation project for overseas talents in Nanjing (R2019LZ05). We thank NASA for providing the NOMAD and VIIRS data. We appreciate the Alfred Wegener Institute Helmholtz Centre for Polar and Marine Research for providing the data sets of SONNE cruise S0202/2 and POLARSTERN cruise ANT-XXVIII/3, and express our gratitude to the investigators for in situ data collection and processing. The data archiving for the marginal seas of China in this study is underway and we plan to use a general repository. The NOMAD data are available online (https://seabass.gsfc.nasa.gov/wiki/NOMAD), the South Atlantic Ocean data in ANT-XXVIII/3 cruise are available online (https://doi.pangaea.de/10.1594/PANGAEA.819614), the Pacific Ocean data in SONNE cruise SO202/2 are available online (https://doi.pangaea.de/10.1594/PANGAEA.804525) and the VIIRS satellite product is available online (https://oceandata.sci.gsfc.nasa.gov/VIIRS-SNPP).

References

Alcântara, E., Watanabe, F., Rodrigues, T., & Bernardo, N. (2016). An investigation into the phytoplankton package effect on the chlorophyll-a specific absorption coefficient in Barra Bonita reservoir, Brazil. *Remote Sensing Letters*, *7*(8), 761–770. doi: 10.1080/2150704X.2016.1185189

Berner, T., Dubinsky, Z., Wyman, K., & Falkowski, P. G. (1989). Photoadaptation and the "Package" Effect in Dunaliella Tertiolecta (Chlorophyceae). *In Journal of Phycology*, 25(1), 70–78. doi: 10.1111/j.0022-3646.1989.00070.x

Bidigare, R. R., Ondrusek, M. E., Morrow, J. H., & Kiefer, D. A. (1990). *In vivo absorption properties of algal pigments*. *1302*, 290–302.

Boatman, T. G., Geider, R. J., & Oxborough, K. (2019). Improving the accuracy of single turnover active fluorometry (STAF) for the estimation of phytoplankton primary productivity (PhytoPP). *Frontiers in Marine Science*, *6*(JUN), 1–16. doi:

10.3389/fmars.2019.00319

Bracher, A., Vountas, M., Dinter, T., Burrows, J. P., R¨ottgers, R., & Peeken, I. (2009). Quantitative observation of cyanobacteria and diatoms from space using PhytoDOAS on SCIAMACHY data. *Biogeosciences, 6*, 751–764. doi: 10.5194/bg-6-751-2009

Brewin, R. J. W., Ciavatta, S., Sathyendranath, S., Skákala, J., Bruggeman, J., Ford, D., & Platt, T. (2019). The Influence of Temperature and Community Structure on Light Absorption by Phytoplankton in the North Atlantic. *Sensors, 19*(19), 4182–4207. doi: 10.3390/s19194182

Brewin, R. J. W., Sathyendranath, S., Jackson, T., Barlow, R., Brotas, V., Airs, R., & Lamont, T. (2015). Influence of light in the mixed-layer on the parameters of a three-component model of phytoplankton size class. *Remote Sensing of Environment, 168*, 437–450. doi: 10.1016/j.rse.2015.07.004

Bricaud, Annick；, Claustre, H., Ras, J., & Oubelkheir, K. (2004). Natural variability of phytoplanktonic absorption in oceanic waters: Influence of the size structure of algal populations. *Journal of Geophysical Research: Oceans*, *109*(11), 1–12. doi: 10.1029/2004JC002419

Bricaud, Annick, Babin, M., Morel, A., & Claustre, H. (1995). Variability in the chlorophyll-specific absorption coefficients of natural phytoplankton: analysis and parameterization. *Journal of Geophysical Research*, *100*(C7), 13321–13332. doi: 10.1029/95jc00463

Bricaud, Annick, Claustre, H., Ras, J., & Oubelkheir, K. (2004). Natural variability of phytoplanktonic absorption in oceanic waters: Influence of the size structure of algal populations. *Journal of Geophysical Research: Oceans*, *109*(11), 1–12. doi: 10.1029/2004JC002419

Ciotti, A. M., Lewis, M. R., & Cullen, J. J. (2002). Assessment of the relationships between dominant cell size in natural phytoplankton communities and the spectral shape of the absorption coefficient. *Limnology and Oceanography*, *47*(2), 404–417. doi: 10.4319/lo.2002.47.2.0404

Clementson and Wojtasiewicz. (2019). Dataset on the in vivo absorption characteristics and pigment composition of various phytoplankton species. *Data in Brief, 25*, 104020. doi: 10.1016/j.dib.2019.104020

Ficek, D., Kaczmarek, S., Stoń-Egiert, J., Woźniak, B., Majchrowski, R., & Dera, J. (2004). Spectra of light absorption by phytoplankton pigments in the baltic; conclusions to be drawn from a gaussian analysis of empirical data. *Oceanologia*, *46*(4), 533–555.

Grabowski J. (1984). Fikobiliproteidy i ich naturalne kompleksy – fikobilisomy (Struktura i migracje energii wzbudzenia elektronowego), Z. Probl. Post. Nauk Roln., 271, 133–152.

Hall D. O., Rao K. K. (1999). Photosynthesis, 6th edn., Cambridge Univ. Press, Cambridge, 214 pp.

He, X., Bai, Y., Pan, D., Tang, J., & Wang, D. (2012). Atmospheric correction of satellite

ocean color imagery using the ultraviolet wavelength for highly turbid waters. *Optics Express*, *20*(18), 20754. doi: 10.1364/oe.20.020754

Hirata, T., Aiken, J., Hardman-Mountford, N., Smyth, T. J., & Barlow, R. G. (2008). An absorption model to determine phytoplankton size classes from satellite ocean colour. *Remote Sensing of Environment*, *112*(6), 3153–3159. doi: 10.1016/j.rse.2008.03.011

Jena, B. (2017). The effect of phytoplankton pigment composition and packaging on the retrieval of chlorophyll-a concentration from satellite observations in the Southern Ocean. *International Journal of Remote Sensing*, *38*(13), 3763–3784. doi: 10.1080/01431161.2017.1308034

John E. O'Reilly, St´ephane Maritorena, M. C. O., David A. Siegel, Toole, D., Menzies, D., Raymond C. Smith, Mueller, J. L., B. Greg Mitchell, Kahru, M., Francisco P. Chavez, Strutton, P., Glenn F. Cota, Stanford B. Hooker, McClain, C. R., Carder, K. L., Frank M¨uller-Karger, Larry Harding, Magnuson, A., David Phinney, … Mary Culver. (2000). SeaWiFS postlaunch calibration and validation analyses, part 3. *NASA Technical Memorandum - SeaWIFS Postlaunch Technical Report Series*, *11*(10), 1–57.

Kirk, J. T. O. (1983). Light and photosynthesis in aquatic ecosystems. *Light and Photosynthesis in Aquatic Ecosystems.* doi: 10.2307/2405114

Kirk J T. (1975). a Theoretical Analysis of the Contribution of Algal Cells To the Attenuation of Light Within Natural. *New Phytologist*, *75*(1), 21–36.

Lee, Z., Carder, K. L., & Arnone, R. A. (2002). Deriving inherent optical properties from water color: a multiband quasi-analytical algorithm for optically deep waters. *Applied Optics*, *41*(27), 5755. doi: 10.1364/ao.41.005755

Lewis, K. M., Mitchell, B. G., van Dijken, G. L., & Arrigo, K. R. (2016). Regional chlorophyll a algorithms in the Arctic Ocean and their effect on satellite-derived primary production estimates. *Deep-Sea Research Part II: Topical Studies in Oceanography*, *130*, 14–27. doi: 10.1016/j.dsr2.2016.04.020

Morel and Bricaud. (1981). Theoretical results concerning light absorption in a discrete medium, and application to specific absorption of phytoplankton. *Deep-Sea Researc*, *28A*(11), 1375–1393. doi: 10.1016/j.jmarsys.2014.09.007

Mouw, C. B., Hardman-Mountford, N. J., Alvain, S., Bracher, A., Brewin, R. J. W., Bricaud, A., Ciotti, A. M., Devred, E., Fujiwara, A., Hirata, T., Hirawake, T., Kostadinov, T. S., Roy, S., & Uitz, J. (2017). A consumer's guide to satellite remote sensing of multiple phytoplankton groups in the global ocean. *Frontiers in Marine Science*, *4*(FEB). doi: 10.3389/fmars.2017.00041

Mouw, C. B., & Yoder, J. A. (2010). Optical determination of phytoplankton size composition from global SeaWiFS imagery. *Journal of Geophysical Research: Oceans*, *115*(12), 1–20. doi: 10.1029/2010JC006337

Nelson, N. B., Prezelinl, B. B., & Robert, R. (1993). Phytoplankton light absorption and the

613 package effect in California coastal waters. *Marine Ecology Progress Series*, *94*(3),
614 217–227.

615 Soppa, M. A., Dinter, T., Taylor, B. B., & Bracher, A. (2013). Satellite derived euphotic
616 depth in the Southern Ocean: Implications for primary production modelling. *Remote*
617 *Sensing of Environment*, *137*, 198–211. doi: 10.1016/j.rse.2013.06.017

618 Sun, D., Huan, Y., Qiu, Z., Hu, C., Wang, S., & He, Y. (2017). Remote-Sensing Estimation
619 of Phytoplankton Size Classes From GOCI Satellite Measurements in Bohai Sea and
620 Yellow Sea. *Journal of Geophysical Research: Oceans*, 8309–8325. doi:
621 10.1002/2017JC013099

622 Sun, D., Huan, Y., Wang, S., Qiu, Z., Ling, Z., Mao, Z., & He, Y. (2019). Remote sensing of
623 spatial and temporal patterns of phytoplankton assemblages in the Bohai Sea, Yellow
624 Sea, and East China Sea. *Water Research*. doi: 10.1016/j.watres.2019.03.081

625 Tarchevsky I. A. (1977). Osnovy fotosinteza, Vyshaya Shkola, Moskva, 256 pp.

626 Taylor, B. B., Torrecilla, E., Bernhardt, A., Taylor, M. H., Peeken, I., Röttgers, R., Piera, J.,
627 & Bracher, A. (2011). Bio-optical provinces in the eastern Atlantic Ocean and their
628 biogeographical relevance. *Biogeosciences Discussions*, *8*(4), 7165–7219. doi:
629 10.5194/bgd-8-7165-2011

630 Wang, G., Lee, Z., & Mouw, C. B. (2018). Concentrations of multiple phytoplankton
631 pigments in the global oceans obtained from satellite ocean color measurements with
632 MERIS. *Applied Sciences (Switzerland)*, *8*(12), 21–24. doi: 10.3390/app8122678

633 Wang, S. Q., Ishizaka, J., Yamaguchi, H., Tripathy, S. C., Hayashi, M., Xu, Y. J., Mino, Y.,
634 Matsuno, T., Watanabe, Y., & Yoo, S. J. (2014). Influence of the changjiang river on the
635 light absorption properties of phytoplankton from the east China sea. *Biogeosciences*,
636 *11*(7), 1759–1773. doi: 10.5194/bg-11-1759-2014

637 Woźniak, B., & Dera, J. (2007). Light absorption in sea water. In Light Absorption in Sea
638 Water (Vol. 33). doi: 10.1007/978-0-387-49560-6

639 Woźniak, B., Dera, J., Ficek, D., Majchrowski, R., Kaczmarek, S., & Koblentz-Mishke, O. I.
640 (1999). Modelling the influence of acclimation on the absorption properties of marine
641 phytoplankton* Phytoplankton absorption Photo-chromatoadaptation Package effect
642 Absorption properties of photoprotecting and photosynthetic pigments. *Oceanologia*,
643 *41*(2), 187–210.

644 Xi, H., Losa, S. N., Mangin, A., Soppa, M. A., Garnesson, P., Demaria, J., Liu, Y., d'Andon,
645 O. H. F., & Bracher, A. (2020). Global retrieval of phytoplankton functional types based
646 on empirical orthogonal functions using CMEMS GlobColour merged products and
647 further extension to OLCI data. *Remote Sensing of Environment*, *240*(February),
648 111704. doi: 10.1016/j.rse.2020.111704

649 Ye, H., Zhang, B., Liao, X., Li, T., Shen, Q., Zhang, F., Zhu, J., & Li, J. (2019). Gaussian
650 decomposition and component pigment spectral analysis of phytoplankton absorption

651 spectra. *Journal of Oceanology and Limnology, 37*(5), 1542–1554. doi: 10.1007/s00343-
652 019-8079-z

653 Zindler, C., Bracher, A., Marandino, C. A., Taylor, B., Torrecilla, E., Kock, A., & Bange, H.
654 W. (2013). Sulphur compounds, methane, and phytoplankton: Interactions along a north-
655 south transit in the western Pacific Ocean. *Biogeosciences, 10*(5), 3297–3311. doi:
656 10.5194/bg-10-3297-2013